ADVANCED FUNCTIONAL MATERIALS
www.afm-journal.de

Bioinspired Lubricated Slippery Magnetic Responsive Microplate Array for High Performance Multi-Substance Transport

Kexiang Shao, Shaojun Jiang, Yanlei Hu, Yiyuan Zhang, Chuanzong Li, Yuxuan Zhang, Jiawen Li, Dong Wu,* and Jiaru Chu*

In nature, many organisms have the ability to transport substances, such as bubbles, droplets, or solids, on demand to meet their survival needs. Inspired by these distinct behaviors, a variety of substance transport strategies have been developed for promising applications in microfluidics, microelectronics, and biomedicine. However, it is still challenging to achieve versatile multi-substance (gas, liquid, and solid) transport. In this work, a triple-biologically inspired lubricated slippery magnetic-responsive microplate array (LS-MMA) by integrating the characteristics of fish scales, Nepenthes peristome, and respiratory cilia is proposed for multi-substance transport. Under the actuation of the moving magnetic field, the microplates bend and overlap sequentially to form a continuous slippery surface with large curvature. With the continuous motion of the slippery surface, active multi-substance transport can be realized. The transport speed of the bubbles, droplets, and solid glass balls can reach ≈5, ≈14, and ≈80 mm s^{-1}, respectively. By virtue of the lubricant's capillary sticking property to the substance, the LS-MMA also realizes 3D on-demand transport of bubbles and droplets. The LS-MMA-based multi-substance transport strategy improves the applicability and flexibility of target manipulation and has a broad potential application in the fields of microchemical reactions and biomedical engineering.

1. Introduction

On-demand transport of multi-substance (i.e., three phase substance gas/liquid/solid) on smart surfaces arouses extensive attention due to the emerging applications in industrial production. For example, bubble manipulation is important in the field of heat transfer, catalytic reactions, and gas flotation.[1] The on-demand droplet manipulation is desired for lab-on-a-chip devices, oil/water separation, water-collecting, and filtration.[2] Controllable transport of solid substance also has alluring prospects in drug delivery, micro-object sorting, and self-cleaning.[3] Till now, researchers have prepared a series of stimulus-responsive surfaces to enable the directional transport of gases, liquids, and solids. The electrowetting surfaces,[2a,3d,4] light-responsive surfaces,[2d,5] thermal-responsive surfaces,[2c,d,6] and magnetic-responsive surfaces[3b,7] have been constructed to realize controllable manipulation. In particular, compared with other stimulus methods, magnetic stimulus has the advantages of remote controllable, battery-free, fast response, and good biosafety, which has been widely used for the controllable substance transport.[2c,d] For example, the lubricant-infused magnetically responsive microcone-structured surface (carpets) can reversibly switch the adhesion state of the bubble or droplet between the pin and slip states by controlling the alignment response of the microcone structures with a traveling magnetic field wave, thus realizing the continuous and controllable manipulation of bubble[7c] or droplet.[7d] By the bending deformation of microstructure or the local dent deformation of elastomer, droplet can be transported by the superhydrophobic magnetically responsive elastomer surface.[7a,8] The lubricating fluid is infused into the magnetically responsive structures to form the slippery liquid-infused porous surface (SLIPS), which allows for the controllable transport of droplets with different surface energies.[9] Ferrofluid can also be infused into the structured surface to construct the magnetically responsive SLIPS. By moving the magnet, the droplet or bubble can be transported by the ferrofluid meniscus formed between the droplet (or bubble) and the ferrofluid-infused surface.[9a,10] Furthermore, solid particles can also be transported by a soft magnetic carpet with soft responsive pillars.[3b,c,11]

Although diverse magnetically responsive surfaces have been developed to realize controlled transport of bubbles, droplets, or solids, there are still some deficiencies: 1) Only active controllable transport of one or two phases substance can be realized.

K. Shao, S. Jiang, Y. Hu, Y. Zhang, Y. Zhang, J. Li, D. Wu, J. Chu
CAS Key Laboratory of Mechanical Behavior and Design of Materials
Key Laboratory of Precision Scientific Instrumentation of
Anhui Higher Education Institutes
Department of Precision Machinery and Precision Instrumentation
University of Science and Technology of China
Hefei 230027, China
E-mail: huyl@ustc.edu.cn; dongwu@ustc.edu.cn
C. Li
School of Instrument Science and Opto-Electronics Engineering
Hefei University of Technology
Hefei 230009, China
The ORCID identification number(s) for the author(s) of this article can be found under https://doi.org/10.1002/adfm.202205831.

DOI: 10.1002/adfm.202205831

The controllable transport of multi-substances (gas, liquid, and solid) remains a challenge. 2) 3D active transport ability of bubbles or droplets is limited. In other words, it is difficult to realize high-performance anti-buoyancy bubble transport or anti-gravity droplet transport. In brief, developing a strategy to achieve active and on-demand 3D transport of multi-substance remains an ultimate challenge.

Natural organisms possessing specific surfaces and functions, which are propitious for their survival and propagation, give us lots of enlightenment to rationally design biomimetic surfaces. Fish scale has multiscale anisotropic rough micro/nano structure, and the surface is covered by a thin layer of mucus.[12] The fan-shaped fish scales are densely arranged and form a slippery surface that has underwater drag reduction and self-cleaning function.[13] Nepenthes has the slippery peristome surface that is fully wetted by water and nectar, enabling efficient capture of insect into the pitcher.[2a,d,14] Respiratory cilia can oscillate in a certain direction to actively transport the pathogens out in order to protect the respiratory system.[3b,c,15]

Herein, inspired by these three biological systems, a kind of multifunctional lubricated slippery magnetic responsive microplate array (LS-MMA) is prepared for the on-demand multi-substance transport (**Figure 1**a). A micro-groove array that imitates the cracked structure of the fish scales is constructed on the magnetic responsive microplate array (MMA), to efficiently store lubricant (silicone oil) infused into the surface. By directional bending under the action of the magnetic field, the microplate array can overlap to form a continuous large-area slippery surface just as the fish skin. Inspired by the function of the peristome surface of the Nepenthes plants, the slippery surface constructed by LS-MMA reduces the object moving resistance and provides high capillary sticking force. Under the moving magnetic field, the microplate array can oscillate like the respiratory cilia, making the slippery surface move continuously and thus realizing the active transport of various objects (Figure 1b–d). With the bionic features mentioned above, the gas bubble, liquid droplet, and solid particle all can be transported by the LS-MMA. Thanks to the active propulsion of the structure and the perpendicular sticking properties of the lubricant to the bubble and droplet, even high-performance anti-buoyancy bubble transport and anti-gravity droplet transport can be achieved.

2. Results and Discussion

2.1. The Fabrication of LS-MMA and Substance Transport

MMA is prepared by a hybrid process combining femtosecond laser writing and soft transfer (**Figure 2**a).[7a,8c] Polytetrafluoroethylene (PTFE) plate is used as the mold for soft transfer. PTFE is a kind of material with low surface energy,[14c,16] which makes Polydimethylsiloxane (PDMS) less likely to adhere to the mold and greatly reduces the difficulty of demold. First, a high aspect ratio groove array is obtained by directly ablating PTFE with femtosecond laser (Figure S1, Supporting Information).

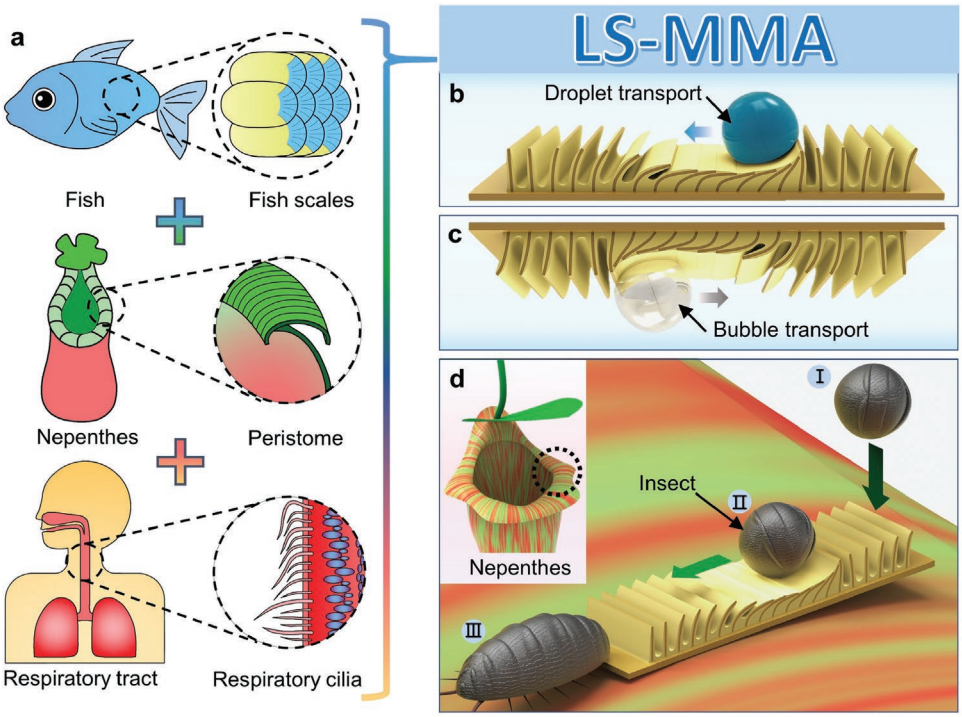

Figure 1. Bio-inspired LS-MMA for multi-substance transport. a) The triple-biologically inspired design of LS-MMA is adopted by combining the cracked structure and the overlapping characteristics of fish scales, the slippery surface of Nepenthes peristome, and the directional transport characteristics of respiratory cilia. b) Schematic of droplet transport with LS-MMA. The object can be transported actively and controllably by the orderly oscillation of the microplate array. c) Schematic of bubble transport with LS-MMA. d) Schematic of insect transport with LS-MMA. Inset shows that the directional transport of live insect is a typical example of solid transport behavior inspired by the Nepenthes peristome.

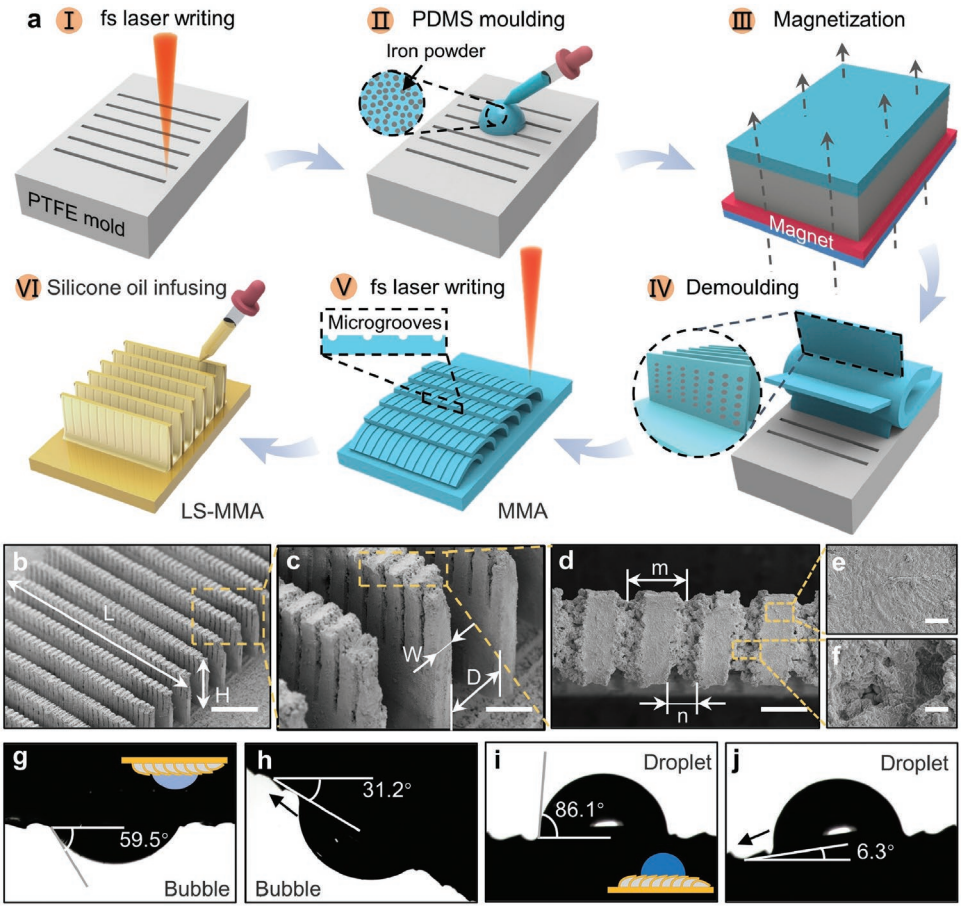

Figure 2. Fabrication process of LS-MMA and its morphological characteristics. a) Schematic of the fabrication process of LS-MMA. b–f) SEM images of LS-MMA. *L* indicates the length of microplate, which is ≈4 mm. *H* indicates the height of microplate, which is ≈1 mm. *D* indicates the space between two microplates, which is ≈0.4 mm. *W* indicates the thickness of microplate, which is ≈95 µm. *m* and *n* indicate the microgroove spacing and radius that are ≈100 µm and ≈50 µm, respectively. Scale bars are (b) 700 µm, (c) 200 µm, (d) 70 µm, and (e, f) 10 µm, respectively. g–j) The images show the contact angle (CA) and sliding angle (SA) of air bubble in water are 59.5° and 31.2°, respectively. And the CA and SA of water droplet in air are 86.1° and 6.3°, respectively. The insets show the contact morphology of bubble and droplet with overlapping lubricated microplates.

Then, the carbonyl iron powder doped liquid PDMS is poured into the PTFE mold. To assemble the iron particles into chains for enhanced magnetic response, the sample is placed on a neodymium-iron-boron (NdFeB) permanent magnet. Carbonyl iron particles are magnetized in the magnetic field and become polar. In this way, they spontaneously arrange in chains along magnetic induction lines.[17] After heating and curing, the iron powder chains are frozen and preserved. The MMA with high aspect ratio (H/W = ≈10.53) can be readily obtained after demolding.

By applying a horizontal magnetic field, all the microplates of the MMA can bend and overlap into a continuous plane. Femtosecond laser is used again to ablate the MMA to form equal space microgrooves on the microplates (Figure 2b–d). Meanwhile, unlike the smooth area of unstructured surface (Figure 2e), the porous structures were induced in the microgroove, which are produced by laser ablation and deposition of splashed particles during ablation (Figure 2f).[18] Then, the lubricating oil (dimethyl silicone oil) is infused into the MMA surface to obtain the LS-MMA. The lubricating oil can spontaneously enter the microstructure and spread across the surface due to the capillary force. Dimethyl silicone oil meets the requirements for creating liquid-infused surfaces:[14b,c,19] 1) Dimethyl silicone oil can wet and stably adhere to PDMS. 2) PDMS substrate is preferentially wetted by the dimethyl silicone oil, rather than by the test liquid. 3) The substances that are soluble with dimethyl silicone oil are limited, so dimethyl silicone oil can be used to repel another substance. Due to the storage of lubricating oil in the porous microgrooves structure, the LS-MMA surface forms a stable, self-healing, lubricating surface like the Nepenthes peristome. The fluidic nature of the lubricating layer means that the dimethyl silicone oil can simply fill the gap between the overlapping microplates by surface-energy-driven capillary action, and form a large area of continuous slippery surface.[14c] Figure 2g–j shows the wetting characteristics on the LS-MMA. The contact angle (CA) and sliding angle (SA) of air bubble are 59.5° and 31.2° respectively, and the CA and SA of water droplet are 86.1° and 6.3°, respectively. Due to the small sliding angle, bubbles and droplets can easily slide on this surface. Meanwhile, the silicone oil layer on the slippery surface also provides a sticking force for solid, ensuring that the solid transport is continuous and the

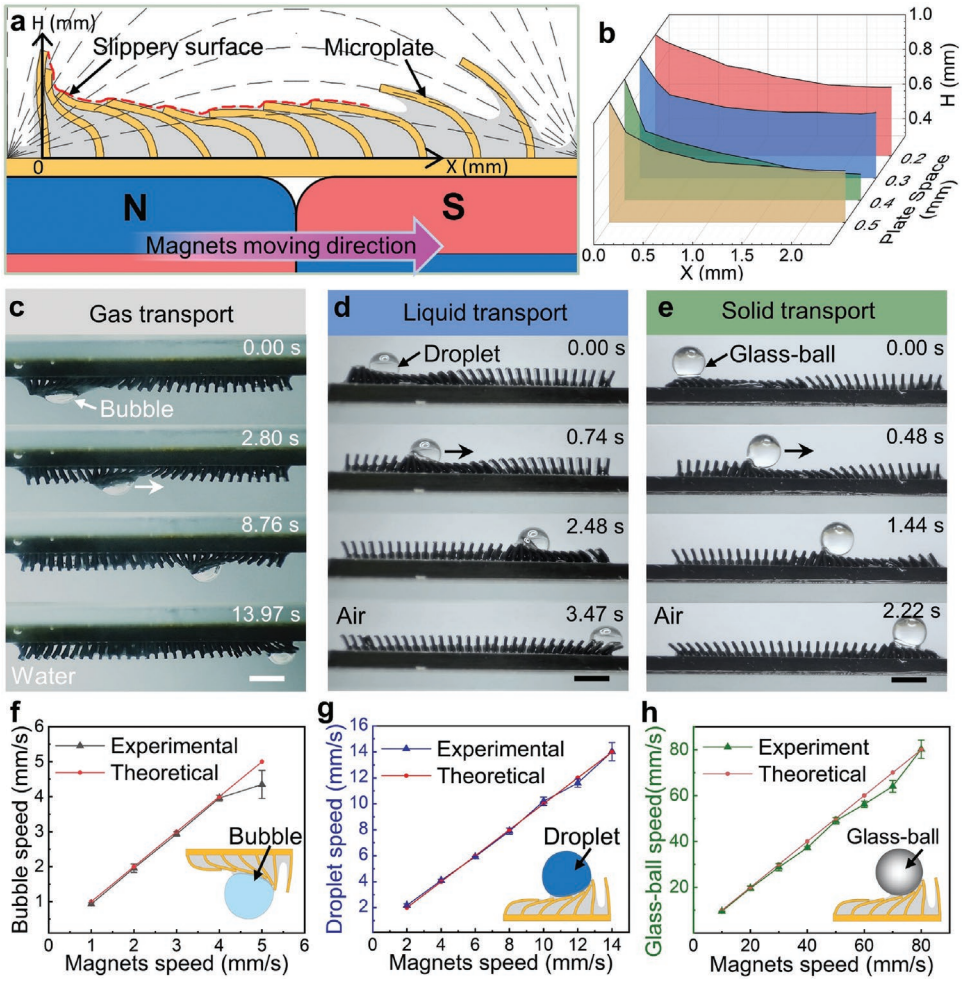

Figure 3. The multi-substance transport with LS-MMA. a) The schematic of magnetic field and microplate bending. The microplates overlap each other to form the large curvature slippery surface. b) The morphology of slippery surface in the *X-H* plane with different microplate space (*D*). When $D = 0.4$ mm, the curvature of slippery surface reaches the maximum. c–e) Optical images of the air bubble (≈3 µL) transport, the water droplet (≈3 µL) transport, and the solid glass-ball (≈3 mm^3) transport, respectively. Scale bar: 2 mm. f–h) Experimental results of the bubble (≈3 µL), droplet (≈3 µL), and glass-ball (≈3 mm^3) transport speed versus magnets speed ($D = 0.4$ mm, $d = 1$ mm). The insets are schematic sketches of the object transport process.

anti-gravity solid transport can be realized (Figures S2, S3, and Video S1, Supporting Information).

When LS-MMA is placed in a magnetic field, the microplate can bend along the magnetic field direction due to the magnetic moment in iron powder chain.[17a,20] The magnetic field around two combined square NdFeB magnets is shown in **Figure 3**a. When the moving platform drives the magnetic field to approach the LS-MMA, the direction of magnetic induction line at the fixed position gradually tends to be horizontal, making the microplates gradually bend. Because the microplate space (*D*) is smaller than the microplate height (H), the adjacent microplates can overlap with each other. The maximum bending angle of the microplate can be reached when the microplate is located above the region of magnetic polarity variation.[7a,17b] As the magnetic field continues to move, the magnetic moment of the magnetic powder chain in the microplate reverses instantaneously. However, because the end of the microplate is pressed by the microplate behind it, this microplate cannot rebound instantly, but gradually upright. At the same time, due to the good flexibility of PDMS, the process of the microplate from maximum bending angle to upright is very short, which ensures a big curvature of the slippery surface (Figure 3a). With the magnets continuous movement, each microplate asymmetrically oscillate in a certain direction, leading to the LS-MMA movement state like respiratory cilia.[15c]

Because of the self-healing property of the scratches on the lubricant infused surface,[14c] discontinuous microplate array can form a large slippery surface like the fish scales when overlapped.[12b] By controlling the microplate space (*D*) and magnets distance (*d*) (Figure S4, Supporting Information), the overlapped surface can be designed. As shown in Figure 3b, when the microplate space is <40% of the microplate height (*H*), the increase of *D* leads to a decrease in the number of overlapping microplates. Thus, the pressed microplates are easier to stand upright, and the curvature of the surface increases. On the contrary, when the *D* is larger than 40% of the *H*, the mutual inhibition effect is greatly reduced because the distance between adjacent microplates is too far, resulting in a decrease in both continuity and curvature of the surface after bending (Figure S5, Supporting Information). The mag-

netic field is controlled to move at a set speed, thus maintaining the motion of the slippery surface and realizing the continuous transport of multi-substance. The air bubble transport in water (Figure 3c), water droplet transport in air (Figure 3d), and glass-ball transport in air (Figure 3e) are carried out as examples of multi-substance on-demand transport (Video S2, Supporting Information).

The object transport speed can be well controlled. The slippery surface moves at the same speed as the magnetic field. So the bubble, droplet, or glass-ball can be transported at almost the same speed as the magnetic field. According to this phenomenon, substances transport speed can be precisely controlled as required. However, when the slippery surface moves too fast, the object can be out of step due to the inertia, resulting in motion failure. The maximum transport speed of bubble, droplet, and glass-ball in horizontal direction are investigated. By gradually increasing the movement speed of the magnetic field, the maximum transport speed of the air bubble (≈3 μL), water droplet (≈3 μL), and glass-ball (≈3 mm^3) can reach ≈5, ≈14, and ≈80 mm s^{-1}, respectively (Figure 3f–h). Compared with the existing magnetic-based substances transport strategies,[2c,e,3a,21] the LS-MMA has higher transport speed and more diverse substances transport capacity.

2.2. Mechanism Analysis for Substance Transport on the LS-MMA

Substance transport is achieved by sequential bending of microplates. As shown in **Figure 4**a, the transport process can be divided into five states according to the experimental observation: I) At first, the magnetic field is far away from the microplate array and the microplates keep upright. The object falls at the top of the microplates 2, 3. II) When the magnetic field approaches LS-MMA, the microplates can gradually bend in turn. III) When LS-MMA is located above the region where the magnetic field polarity changes, the bending angle of the microplate reaches the maximum. The microplates overlap to form a continuous slippery surface. Droplet or bubble floats well on the sides of microplates 2, 3, and 4 due to the liquid repellency of the lubricated surface. IV) When the magnetic field polarity change area passes by, the microplate 2 has a sudden rebound tendency. Due to the end being pressed by the adjacent microplate, microplate 2 is not fully upright but slightly raises at the top. Microplates 2, 3, and 4 form a continuous large curvature slippery surface. The object is driven by gravity and microplate thrust. V) As the magnets continue to move, the microplates 1, 2, and 3 are gradually lifted and turn upright, and finally bend backward along the magnetic induction line. Then, the microplate 4 and 5 repeat the above steps to achieve continuous movement of the slippery surface. The object follows this motion process to the microplates 4 and 5, eventually realizing continuous transport (Video S2, Supporting Information).

In order to obtain the best transport performance, the parameters affecting the transport capacity are discussed separately. First, the microplate space (D) significantly affects the maximum transport speed (Figure S6, Supporting Information). Figure 4b–d shows the influence of microplate space on the maximum transport speed of objects. When D is <40% (≈0.4 mm) of the microplate height (H, ≈1 mm) the maximum speed of object transport increases with D. When D is >40% of H, the maximum speed of object transport decreases with the increase of D. Consistent with the above analysis, the increase of the surface curvature undoubtedly increases the component of the microplate impact force in the direction of motion and thus improves the motion ability. However, the decrease of surface continuity obviously increases the resistance of the object transport. In addition, the volume of the object is also an important factor (Figure 4e–g; Figure S7, Supporting Information). For bubble and droplet, objects with larger volume need a larger area of lubricating surface to support, so the maximum transportable volume of bubble and droplet is limited by the size of microplate. For solid transport, massive object requires bigger driving force to overcome inertia, and their maximum transportable volume is limited by the maximum driving force that can be provided by the LS-MMA. At the same time, larger objects bring greater resistance during rapid transport, which further limits the transport ability of LS-MMA. LS-MMA has high efficiency in transporting tiny droplets and bubbles (<3 μL), which have potential applications in microchemical reactions and bioassays.[22] The external magnetic field, which is the source of driving force is also an important parameter (Figure S8, Supporting Information). Higher magnetic field intensity makes the magnetic-responsive microplates bend more easily, and increases the curvature of the slippery surface. By controlling the distance (d) between the magnets and the microplate, the maximum object transport speed under different magnetic field intensities is tested (Figure 4h–j; Figure S4, Supporting Information). Experiments show that when the magnetic field intensity is >100 mT, the maximum speed of object transport is basically stable. However, when the magnetic field intensity is <100 mT, the bending angle of microplate decreases obviously, resulting in the insufficient driving force and the decrease of transport capacity. Despite the different maximum transport speed for different substances, it is worth noting that the maximum transport speeds of bubble, droplet, and glass-ball have the same change trend. In general, the maximum transport speed of glass-ball is greater than droplet. And the maximum transport speed of droplet is greater than bubble. The transport speed differences should be related to the contact angle (CA) and sliding angle (SA) of various substances on the slippery surface.

The forces on the object during transport are further analyzed. As shown in Figure 4k–m, the forces on the object are simplified into four external forces, and the F_{Driving} is the resultant force in the motion direction.[8c,9a,23] Bubble transport can be realized under the following conditions:

$$F_{\text{Driving}} = F_{\text{plate}} \cos\alpha - F_{\text{Buoyancy}} \sin\beta - f > 0 \quad (1)$$

where F_{plate} is the force of the microplate array acting on the object, and its direction is perpendicular to the tangential direction of the maximum curvature position of the surface. α is the angle between the microplate force F_{plate} and the motion direction, which is related to the magnetic field intensity and the microplate space (D). F_{Buoyancy} is the buoyancy force of the bubble, whose magnitude is $F_{\text{Buoyancy}} = \rho g V$ (where ρ, g, and V

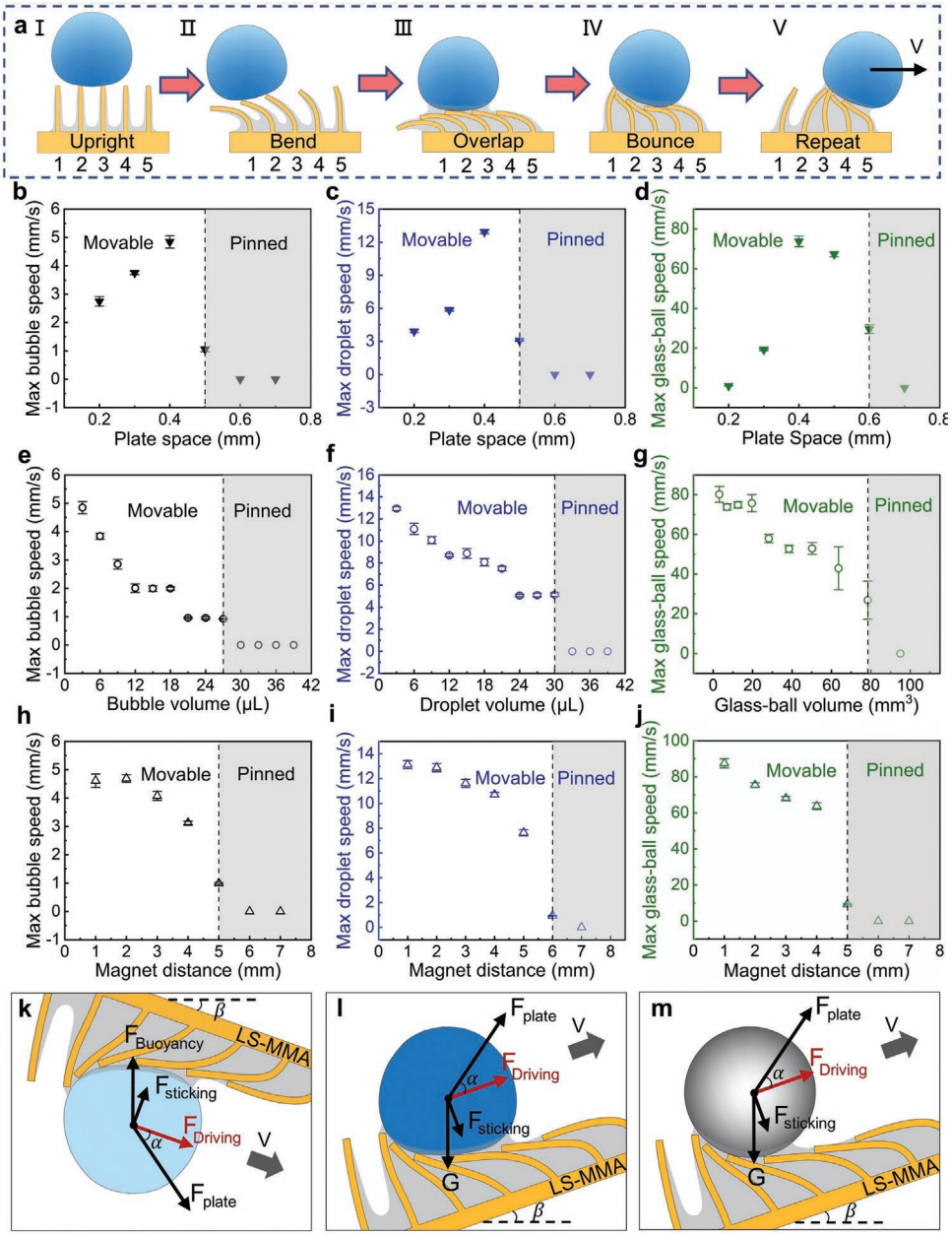

Figure 4. Object transport mechanism of the LS-MMA surface. a) Schematic of the object horizontal transport process under external magnetic field excitation. b–d) Experimental results of the maximum transport speed of bubble (≈3 μL), droplet (≈3 μL), and glass-ball (≈3 mm³) versus microplate space (with the same magnets distance $d = 1$ mm). When the microplate space is 0.4 mm, LS-MMA has the best transport performance. e–g) Experimental results of the maximum transport speed of bubble, droplet, and glass-ball versus objects volume ($D = 0.4$ mm, $d = 1$ mm). h–j) Experimental results of the maximum transport speed of bubble (≈3 μL), droplet (≈3 μL), and glass-ball (≈3 mm³) versus magnets distance ($V = 3$ μL, $D = 0.4$ mm). When the magnets distance is <0.4 mm, the maximum transport speed of objects remains stable at a high value. k–m) The force analysis of bubble transport in water, droplet transport in air, and glass-ball transport in air, respectively.

are the environmental liquid density, acceleration of gravity, and bubble volume, respectively). And the direction is perpendicular to the ground upward. β is the angle between the motion direction and the horizontal plane. f is the object transport resistance. The forces of droplet or solid have a similar form, expressed as:

$$F_{\text{Driving}} = F_{\text{plate}} \cos\alpha - G \sin\beta - f > 0 \quad (2)$$

where G is the gravity of the droplet or solid, whose magnitude is $G = \rho g V$ (where ρ, g, and V are the object density, acceleration of gravity, and object volume, respectively), perpendicular to the ground downward. At the same time, the resultant force perpendicular to the motion direction ensures that the object does not separate from the surface during transport, so the forces on the bubble should also meet the following requirements:

$$F_{plate}\sin\alpha - F_{Buoyancy}\cos\beta - F_{sticking} < 0 \quad (3)$$

Droplet or solid should satisfy the relation:

$$F_{plate}\sin\alpha - G\cos\beta - F_{sticking} < 0 \quad (4)$$

where $F_{sticking}$ is the sticking force between the object and the slippery surface. Because the dimethyl silicone oil (350 CS) used in this experiment provide a stable liquid layer, the capillary forces bring a potential to adhere the object.[24] On the premise of object does not separate from the surface, the greater the driving force is, the faster object moves. Among them, the stronger magnetic field intensity provides the larger F_{plate}, the larger curvature of the slippery surface provides the smaller α, and the smaller transport slope provides the smaller β. All these factors have positive effect on the $F_{Driving}$, which is consistent with the experimental results above. On the other hand, for the fixed magnetic field intensity and microplate array size, the forces of the object have fixed F_{plate} and α. If $F_{sticking}$ is large enough, driving force can be generated at any β angle, which provides the possibility for anti-buoyancy and anti-gravity transport of objects.

2.3. Anti-Buoyancy Bubble Transport, Anti-Gravity Droplet Transport, and Anti-Gravity Solid Transport by LS-MMA

For traditional on-demand substance transport strategies by stimulus-responsive surfaces, the full-angle anti-buoyancy transport of bubble and anti-gravity transport of droplet are challenging to achieve. The anti-gravity solid transport at big slope angle is also challenging.[5b,6b,7c,8a,9a] Because the adhesion of droplet or solid is ultralow on superhydrophobic surfaces, gravity prevents the upward movement of object (Figure S9a, Supporting Information). Similarly, the transport method using buoyancy as a driving force has difficulty in bubble subsidence. In this work, LS-MMA can realize anti-buoyancy bubble transport and anti-gravity droplet transport. On the vertical surface (β = 90°), the bubble can be sunk at ≈1 mm s^{-1} (**Figure 5**a), and the droplet can be upraised at ≈1 mm s^{-1} (Figure 5b). And the solid glass-ball can be transported at ≈1 mm s^{-1} at β = 30° (Figure S9b, Supporting Information). This phenomenon is attributed to the larger curvature of the slippery surface, resulting in a smaller α, so that F_{plate} can overcome buoyancy or gravity to produce $F_{Driving}$, which is consistent with the above mechanics analysis. Furthermore, the bubble and droplet can still be transported at a speed of ≈1 mm s^{-1} when β = 180°. This is mainly due to the capillary sticking force of the lubricant to the substance, ensuring that objects cannot be separated from the LS-MMA by gravity or buoyancy (Figure S10, Supporting Information). Different from the most transport strategies that utilize gravity or buoyancy as the driving force, LS-MMA can realize the full-angle (0°–360°) active transport of bubble and droplet, and the big slope angle (30°) anti-gravity solid transport (Videos S3 and S4, Supporting Information).

2.4. Complex Substances Transport and Microchemical Reactions by LS-MMA

Due to the liquid repellent characteristics of the dimethyl silicone oil, the LS-MMA has ability to transport complex

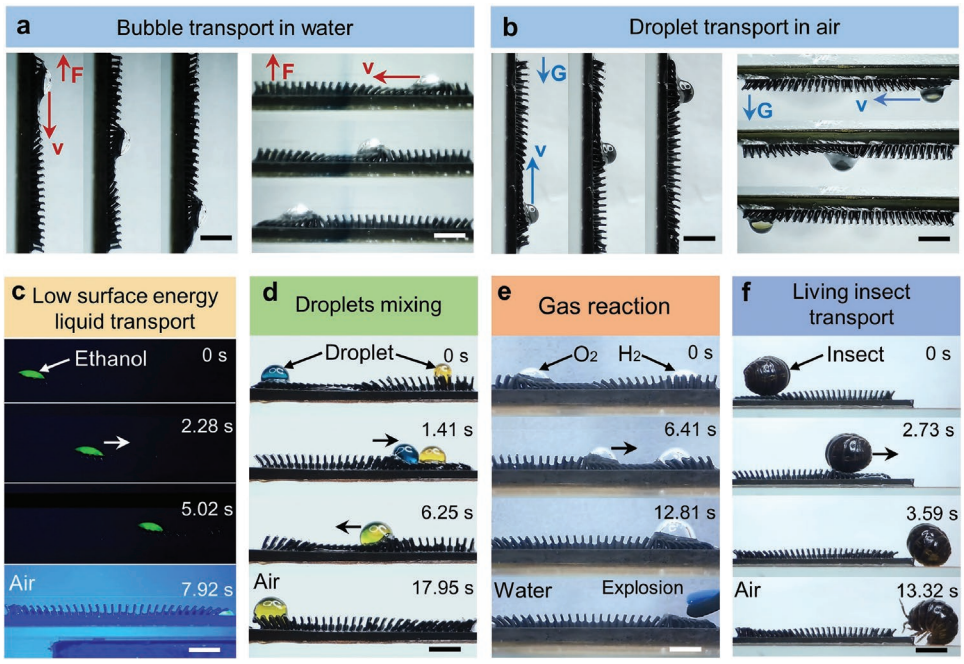

Figure 5. 3D full-angle active transport and multifunctional applications of LS-MMA. a,b) Optical images of an air bubble (3 µL) and a water droplet (3 µL) transport with LS-MMA when β = 90° and 180°, respectively. The bubble can be transported anti-buoyancy and the droplet can be transported anti-gravity. c) Optical fluorescence images of the low surface energy liquid droplet (ethanol, m% = 75%, 3 µL) transport with LS-MMA. The last image (7.92 s) was taken in the bright field. d) Optical images of on-demand merging and fast mixing of water droplets (3 µL) with LS-MMA. e) Optical images of a gas reaction based on the microbubble horizontal transport. O_2 bubble (3 µL) is transported to the right and merged with H_2 bubble (6 µL). The mixed gas can be exploded by the electric spark. f) Optical images of an active directional transport of a living insect (pill worm). Scale bar: (a–e) 2 mm, (f) 3 mm.

liquid.[14c,22] As a biomedical application demonstration, LS-MMA is used to transport medical glucose solution (Figure S11 and Video S5, Supporting Information). Moreover, LS-MMA can be used to transport low surface tension droplet (Figure S12, Supporting Information). Figure 5c shows the successful transport for the medical ethanol solution droplet (m% = 75%, surface tension ≈24.5 mN m^{-1}, 25 °C)[25] by LS-MMA (Video S6, Supporting Information). By fluorescent staining of the droplet, it is observed that no leakage occurred during ethanol solution droplet transport. However, it is difficult for the previously reported superhydrophobic surface-based droplet manipulation strategies to transport such a low surface energy liquid. The mixing of droplets or bubbles is the main form of microchemical reactions. Substance transport strategies using magnetic excitation have the advantages of remote control and fast response that can be used to achieve contactless microchemical reactions.[7a,c] As shown in Figure 5d, LS-MMA can be used for on-demand merging and fast mixing of microdroplets. Two droplets are merged under the drive of the microplates. And the mixing process can be accelerated by reciprocating motions of the slippery surface (Video S7, Supporting Information). Not limited to liquid substances, Figure 5e shows the active and controlled merging of a hydrogen bubble and an oxygen bubble in a water environment by LS-MMA. The mixed gas can be exploded by the electric spark generated by the piezoelectric ceramic (Video S8, Supporting Information). Imitating the Nepenthes feeding process, the live pill worm insect can be transported using LS-MMA (Figure 5f; Video S9, Supporting Information). Pill worm remains active after transport. The living insect transport capability of LS-MMA can be applied in biomedical field. Liquid metal as a special liquid substance, is easily oxidized in air, which makes it difficult to be transported.[26] LS-MMA can be used to manipulate the liquid metal at liquid environmental (NaOH solutions) (Figure S11 and Video S10, Supporting Information). In brief, based on the liquid repellent of slippery surface and high sticking force of the lubricant to the substance, combined with the magnetic control reconfigurable surface of LS-MMA, multi-substance transport can be realized.

3. Conclusion

In conclusion, inspired by the cracked structure and overlapping characteristics of fish scales, the slippery liquid-infused surface of Nepenthes peristome, and directional transport ability of respiratory cilia, a kind of lubricated slippery magnetic responsive microplate array is fabricated based on femtosecond laser direct writing, soft transfer, and lubricant infusion. LS-MMA possesses the promising function of multi-substance transport. On horizontal platforms, the typical bubble and droplet of ≈3 µL can be transported in ≈5 and ≈14 mm s^{-1}, respectively, and the typical solid glass-ball of ≈3 mm^3 can be transported at a speed of 80 mm s^{-1}. The maximum transport volume of bubble, droplet, and glass-ball can reach ≈27 µL, ≈30 µL, and ≈79 mm^3, respectively. On this basis, LS-MMA can realize full-angle active transport of bubble and droplet in the vertical plane, which overcomes the limitation of single direction of traditional transport strategies that rely on buoyancy, gravity, or wetting gradient force. In addition, by adjusting the manufacturing parameters of LS-MMA, the curvature of slippery surface can be designed, which further expands its practicability. This work on active transport of multi-substances provides new insights into the development of microfluidics, microchemical reactions, and biomedical detection.

4. Experimental Section

The Fabrication of LS-MMA: The LS-MMA was prepared by soft transfer method using polydimethylsiloxane (PDMS, Sylgard 184, Dow Corning) and carbonyl iron powder (diameter of 3–5 µm, purity ≥99.9%, C = 40%, RuiTeng Alloy Material Co., Ltd.). The laser beam (central wavelength of 800 nm, repetition rate of 1 kHz, pulse width of 104 fs) from a regenerative amplified Ti: sapphire femtosecond laser system (Legend Elite-1K-HE, Coherent, USA) was used in this experiment. The laser beam was focused on the PTFE plate (average thickness of ≈1 mm, Shanghai Huguan Packing Material Co., Ltd.) and MMA by the telecentric f-theta lens (focused length of 63 mm). The fabrication process of LS-MMA is shown in Figure 2a and consists of the following six steps: I) A series of high aspect ratio grooves were ablated on PTFE plate by femtosecond laser rapid writing technique (laser power 500 mW, scanning speed 20 mm s^{-1}, scanning repetition 500 circles). The PTFE mold with a release agent (mesoAnti-2000, Wuhan Jieguan Biotechnology Co., Ltd.) was saturated, and then the surface was blow dried thoroughly with an air gun. A negative PTFE mold was obtained. II) Before PDMS moulding, double-sided tape (Kapton, TED PELLA Inc., USA) was carefully stuck to one side of the mold. Liquid polydimethylsiloxane was mixed with carbonyl iron powder in a weight ratio of 70%, after thoroughly mixing, the cross-linker was added at a ratio of 10:1 (w/w). A degassing procedure was followed to make the mixture to fill the groove. III) In order to obtain the strong magnetic responsive, a permanent magnet of NdFeB (40 × 40 × 20 mm, Shanghai Ze He Mechanical & electrical Co., Ltd.) was placed below the sample for ≈5 s to assemble the iron powder into chains. IV) The sample was placed in an oven at 100 °C for 30 min for curing. The distribution of carbonyl iron powder in the microplate was permanently frozen. After the sample was cooled, the magnetic responsive microplate array (MMA) could be peeled off from the PTFE mold. V) The MMA was placed in a transverse magnetic field, so that all the microplates bended in the same direction, and then the femtosecond laser (laser power 300 mW, scanning speed 15 mm s^{-1}, scanning repetition 1 circle) was used to manufacture the microgrooves on the microplate (groove radius ≈0.05 mm and spacing ≈0.1 mm). Then, the magnetic field was adjusted to switch the bending direction of the microplate, and the step V was repeated. VI) Dimethyl silicone oil (350 CS, Dow Corning) was infused into the MMA surface. The microplate was driven by the magnetic field to extrude the excess dimethyl silicone oil, so that the dimethyl silicone oil was stored in the microgroove and microporous. Finally, the lubricated slippery magnetic responsive microplate array (LS-MMA) could be obtained.

Magnetic Field Drive Equipment: Two NdFeB permanent magnets (15 × 15 × 10 mm, Lanxi Ou Cheng Magnetic Industry Co., Ltd.) were placed side by side to provide the magnetic field to drive the microplate to bend. LS-MMA was glued to a fixed glass supporting base. The permanent magnets were installed on a ball screw platform. During the experiment, when the bubbles, droplets, or solids fell on the surface of LS-MMA, the active transport of the object could be realized by moving the ball screw platform.

Characterization: The topographies of LS-MMA were characterized by using a secondary electron SEM (ZEISS EVO18). A CA100C contact-angle system (Innuo, China) was used to measure the CAs and SAs of the air bubble and water droplet (≈3 µL). A high-speed charge-coupled device camera (120 fps, MER-030120UM/UC, China Daheng Group, Inc.) was used to record the LS-MMA bending deformation and the object transport process under the action of magnetic field. A digital Gauss

meter (HM-100, Huaming instrument Co., Ltd., China) was used to measure the magnetic flux density.

Supporting Information

Supporting Information is available from the Wiley Online Library or from the author.

Acknowledgements

K.S. and S.J. contributed equally to this work. This work was supported by the National Natural Science Foundation of China (Nos. 61927814, 52122511, U20A20290, 52005475, and 52105492), Major Scientific and Technological Projects in Anhui Province (201903a05020005), the Fundamental Research Funds for the Central Universities (WK2090000035). The authors acknowledge the Experimental Center of Engineering and Material Sciences at USTC for the fabrication and measuring of samples. This work was partly carried out at the USTC Center for Micro and Nanoscale Research and Fabrication.

Conflict of Interest

The authors declare no conflict of interest.

Data Availability Statement

The data that support the findings of this study are available from the corresponding author upon reasonable request.

Keywords

3D transport, lubricated slippery surfaces, magnetic-responsive structures, multi-substance transport

Received: May 23, 2022
Revised: July 13, 2022
Published online:

[1] a) X. Wang, H. Bai, J. Yang, Z. Li, Y. Wu, C. Yu, L. Jiang, M. Cao, *Small* **2021**, *17*, 2007803; b) H. Ma, M. Cao, C. Zhang, Z. Bei, K. Li, C. Yu, L. Jiang, *Adv. Funct. Mater.* **2018**, *28*, 1705091; c) C. Yu, X. Zhu, M. Cao, C. Yu, K. Li, L. Jiang, *J. Mater. Chem. A* **2016**, *4*, 16865; d) S. Zhu, Y. Bian, T. Wu, E. Li, J. Li, Y. Hu, D. Wu, J. Chu, *Appl. Phys. Lett.* **2020**, *116*, 093706.

[2] a) Z. Hao, W. Li, *Nanomaterials* **2021**, *11*, 801; b) J. Yong, Q. Yang, C. Guo, F. Chen, X. Hou, *RSC Adv.* **2019**, *9*, 12470; c) P. Lv, Y. L. Zhang, D. D. Han, H. B. Sun, *Adv. Mater. Interfaces* **2021**, *8*, 2100043; d) H. Dai, Z. Dong, L. Jiang, *Science Advanced* **2020**, *6*, eabb5528; e) F. Lv, F. Zhao, D. Cheng, Z. Dong, H. Jia, X. Xiao, D. Orejon, *Adv. Colloid Interface Sci.* **2022**, *299*, 102564; f) Y. Zhao, Y. Su, X. Hou, M. Hong, *Opto-Electronic Advances* **2021**, *4*, 210008.

[3] a) C. Li, S. Wang, M. Liu, Z. Peng, B. Zhang, S. Chen, *ACS Appl. Mater. Interfaces* **2021**, *13*, 37655; b) A. F. Demirors, S. Aykut, S. Ganzeboom, Y. A. Meier, R. Hardeman, J. de Graaf, A. Mathijssen, E. Poloni, J. A. Carpenter, C. Unlu, D. Zenhausern, *Adv. Sci.* **2021**, *8*, 2102510; c) S. Ben, J. Tai, H. Ma, Y. Peng, Y. Zhang, D. Tian, K. Liu, L. Jiang, *Adv. Funct. Mater.* **2018**, *28*, 1706666; d) B. Dai, S. Li, T. Xu, Y. Wang, F. Zhang, Z. Gu, S. Wang, *ACS Appl. Mater. Interfaces* **2018**, *10*, 42979.

[4] a) I. Oh, C. Keplinger, J. Cui, J. Chen, G. M. Whitesides, J. Aizenberg, Y. Hu, *Adv. Funct. Mater.* **2018**, *28*, 1802632; b) J. Cao, Q. An, Z. Liu, M. Jin, Z. Yan, W. Lin, L. Chen, P. Li, X. Wang, G. Zhou, L. Shui, *Sens. Actuators, B* **2019**, *291*, 470.

[5] a) W. Q. Ye, Y. Y. Wei, D. N. Wang, C. G. Yang, Z. R. Xu, *Lab Chip* **2021**, *21*, 1131; b) W. Li, X. Tang, L. J. S. A. Wang, *Science Adv.* **2020**, *6*, eabc1693; c) A. Diguet, R. M. Guillermic, N. Magome, A. Saint-Jalmes, Y. Chen, K. Yoshikawa, D. Baigl, *Angew. Chem. Int. Ed. Engl.* **2009**, *48*, 9281.

[6] a) C. Chen, L. Zhou, L. A. Shi, S. Zhu, Z. Huang, C. Xue, J. Li, Y. Hu, D. Wu, J. Chu, *ACS Appl. Mater. Interfaces* **2020**, *12*, 1895; b) C. Chen, Z. Huang, L. A. Shi, Y. Jiao, S. Zhu, J. Li, Y. Hu, J. Chu, D. Wu, L. Jiang, *Adv. Funct. Mater.* **2019**, *29*, 1904766.

[7] a) S. Jiang, Y. Hu, H. Wu, R. Li, Y. Zhang, C. Chen, C. Xue, B. Xu, W. Zhu, J. Li, D. Wu, J. Chu, *Nano Lett.* **2020**, *20*, 7519; b) J. Wang, Z. Zhu, P. Liu, S. Yi, L. Peng, Z. Yang, X. Tian, L. Jiang, *Adv. Sci. (Weinh)* **2021**, *8*, 2103182; c) K. Han, K. Yong, *Adv. Funct. Mater.* **2021**, *31*, 2101970; d) A. F. Demirors, S. Aykut, S. Ganzeboom, Y. A. Meier, E. Poloni, *Proc. Natl. Acad. Sci. USA* **2021**, *118*, e2111291118.

[8] a) G. Chen, Z. Dai, S. Li, Y. Huang, Y. Xu, J. She, B. Zhou, *ACS Appl. Mater. Interfaces* **2021**, *13*, 1754; b) Y. Lin, Z. Hu, M. Zhang, T. Xu, S. Feng, L. Jiang, Y. Zheng, *Adv. Funct. Mater.* **2018**, *28*, 1800163; c) Y. Song, S. Jiang, G. Li, Y. Zhang, H. Wu, C. Xue, H. You, D. Zhang, Y. Cai, J. Zhu, W. Zhu, J. Li, Y. Hu, D. Wu, J. Chu, *ACS Appl. Mater. Interfaces* **2020**, *12*, 42264.

[9] a) S. Zhu, Y. Bian, T. Wu, C. Chen, Y. Jiao, Z. Jiang, Z. Huang, E. Li, J. Li, J. Chu, Y. Hu, D. Wu, L. Jiang, *Nano Lett.* **2020**, *20*, 5513; b) J. Guo, D. Wang, Q. Sun, L. Li, H. Zhao, D. Wang, J. Cui, L. Chen, X. Deng, *Adv. Mater. Interfaces* **2019**, *6*, 1900653; c) P. Guo, Z. Wang, L. Heng, Y. Zhang, X. Wang, L. Jiang, *Adv. Funct. Mater.* **2019**, *29*, 1808717; d) W. Chen, X. Zhang, S. Zhao, J. Huang, Z. Guo, *Chem. Commun. (Camb)* **2022**, *58*, 1207.

[10] V. Nasirimarekani, F. Benito-Lopez, L. Basabe-Desmonts, *Adv. Funct. Mater.* **2021**, *31*, 2100178.

[11] S. Ben, J. Yao, Y. Ning, Z. Zhao, J. Zha, D. Tian, K. Liu, L. Jiang, *Sci. China: Chem.* **2020**, *63*, 347.

[12] a) Y. Cai, L. Lin, Z. Xue, M. Liu, S. Wang, L. Jiang, *Adv. Funct. Mater.* **2014**, *24*, 809; b) S. Wang, K. Liu, X. Yao, L. Jiang, *Chem. Rev.* **2015**, *115*, 8230.

[13] a) K. Liu, L. Jiang, *ACS Nano* **2011**, *5*, 6786; b) W. Rong, H. Zhang, T. Zhang, Z. Mao, X. Liu, K. Song, *Adv. Eng. Mater.* **2020**, *23*, 2000821.

[14] a) J. Li, J. Li, J. Sun, S. Feng, Z. Wang, *Adv. Mater.* **2019**, *31*, 1806501; b) X. Zeng, Z. Guo, W. Liu, *Bio-Des. Manuf.* **2021**, *4*, 506; c) T. S. Wong, S. H. Kang, S. K. Tang, E. J. Smythe, B. D. Hatton, A. Grinthal, J. Aizenberg, *Nature* **2011**, *477*, 443.

[15] a) S. Ben, T. Zhou, H. Ma, J. Yao, Y. Ning, D. Tian, K. Liu, L. Jiang, *Adv. Sci. (Weinh)* **2019**, *6*, 1900834; b) S. Zhang, Z. Cui, Y. Wang, J. M. J. den Toonder, *Lab Chip* **2020**, *20*, 3569; c) N. Bruot, P. Cicuta, *Annu. Rev. Condens. Matter Phys.* **2016**, *7*, 323.

[16] D. Chu, S. C. Singh, J. Yong, Z. Zhan, X. Sun, J. A. Duan, C. Guo, *Adv. Mater. Interfaces* **2019**, *6*, 1900550.

[17] a) A. C. Liu, J. H. Gillen, S. R. Mishra, B. A. Evans, J. B. J. S. A. Tracy, *Science Advanced* **2019**, *5*, eaaw2897; b) S. Jiang, Y. Hu, H. Wu, Y. Zhang, Y. Zhang, Y. Wang, Y. Zhang, W. Zhu, J. Li, D. Wu, J. Chu, *Adv. Mater.* **2019**, *31*, 1807507.

[18] J. Yong, F. Chen, J. Huo, Y. Fang, Q. Yang, J. Zhang, X. Hou, *Nanoscale* **2018**, *10*, 3688.

[19] C. Zhang, S. Adera, J. Aizenberg, Z. Chen, *ACS Appl. Mater. Interfaces* **2021**, *13*, 15901.

[20] M. M. Schmauch, S. R. Mishra, B. A. Evans, O. D. Velev, J. B. Tracy, *ACS Appl. Mater. Interfaces* **2017**, *9*, 11895.

[21] X. Gou, Z. Guo, *Chem. Eng. J.* **2021**, *411*, 128495.
[22] Y. Zhang, J. Li, L. Xiang, J. Wang, T. Wu, Y. Jiao, S. Jiang, C. Li, S. Fan, J. Zhang, H. Wu, Y. Zhang, Y. Bian, K. Zhao, Y. Peng, W. Zhu, J. Li, Y. Hu, D. Wu, J. Chu, Z. Wang, *Adv. Mater.* **2022**, *34*, 2108567.
[23] C. Yu, X. Zhu, K. Li, M. Cao, L. Jiang, *Adv. Funct. Mater.* **2017**, *27*, 1701605.
[24] J. D. Glover, J. T. Pham, *Soft Matter* **2020**, *16*, 5812.
[25] G. Vazquez, E. Alvarez, J. M. Navaza, *J. Chem. Eng. Data* **1995**, *40*, 611.
[26] B. Ma, C. Xu, J. Chi, J. Chen, C. Zhao, H. Liu, *Adv. Funct. Mater.* **2019**, *29*, 1901370.